Studies of Carbon Nanotubes and Fluorinated Nanotubes by X-ray and Ultraviolet Photoelectron Spectroscopy

Yu-Qing Wang and Peter M. A. Sherwood*

Department of Chemistry, 111 Willard Hall, Kansas State University, Manhattan, Kansas 66506-3701

Received March 30, 2004. Revised Manuscript Received September 13, 2004

Carbon single-walled nanotubes (SWNTs) and fluorinated SWNTs (F-SWNTs) were investigated by core and valence band X-ray photoelectron spectroscopy (XPS) and ultraviolet photoelectron spectroscopy (UPS). The core spectra were interpreted by chemical shift calculations based upon CNDO calculations, and the valence band spectra were calculated using ab initio molecular orbital calculations. Both calculations used various molecules representing different structural models for SWNTs and F-SWNTs. Core XPS studies of SWNTs showed carbon and small amounts of chemisorbed oxygen, while F-SWNTs showed a C 1s region split into four principal components with peaks shifted by 1.25, 4.00, and 7.20 eV from the principal carbon peak. The valence band showed characteristic features that could be interpreted by calculated spectra. The model for SWNTs consisted of a carbon framework with terminating hydrogen atoms. This study indicates that it is possible to see significant differences in the photoelectron spectra for different nanotube structures, especially in the case of fluorinated nanotubes. The fluorinated nanotubes of this study give the best agreement with the calculated spectra for an armchair arrangement nanotube.

Introduction

The discovery of carbon nanotubes by Iijima[1] in 1991 and a method for the large-scale synthesis of nanotubes by Ebbesen and Ajayan[2,3] in 1992 have opened up a new era in materials science and nanotechnology.[3] Since then, various nanotubes, with or without encapsulated metals and having straight, curved, planar-spiral, and single- and double-helical shapes, have been experimentally produced either by the carbon arc method or by pyrolysis of organic chemicals. These elongated nanotubes consist of carbon hexagons arranged in a concentric manner, with both ends of the tubes normally capped by fullerene-like structures containing pentagons. They usually have a diameter on the order of tens to hundreds of angstroms and a length of up to several micrometers and can exhibit semiconducting or metallic behavior depending on their diameter and helicity of the arrangement of graphitic rings in the walls.[4,5] Dissimilar carbon nanotubes may be joined together, allowing the formation of molecular wires with interesting electrical, magnetic, nonlinear optical, and mechanical properties attractive for a variety of potential applications.[6−11]

New nanotubes with potentially novel applications have been prepared by the introduction of various chemical functional groups on the surface of the tube, and the introduction of other elements into the tube structure.[12−15] Plasma process and wet (or dry) chemical oxidation procedures have commonly been employed for surface modification. Generally, gas-phase treatment preferentially forms hydroxyl and carbonyl groups, while liquid-phase treatment forms carboxylic acid groups on the surface in an oxidation process.

Fluorination of single-wall carbon nanotubes (SWNTs) has been reported by Margrave and colleagues[16] and others[17−21] to modify the chemistry by introducing fluorine into the nanotube structure. The process not only changed the surface chemistry of SWNTs, but drastically changed the electronic properties of them,

* Corresponding author. E-mail: peter.sherwood@okstate.edu. Present address: Department of Chemistry, 107 Physical Science I, Oklahoma State University, Stillwater, OK 74078-3071.

(1) Iijima, S. *Nature* **1991**, *354*, 56.
(2) Ebbesen, T. W.; Ajayan, P. M. *Nature* **1992**, *358*, 220.
(3) Dresselhaus, M. S.; Deesselhaus, G.; Eklund, P. *Science of Fullerenes and Carbon Nanotubes*; Academic Press: New York, 1996.
(4) Ebbsen, T. *Carbon Nanotubes*; CRC Press: Boca Raton, FL, 1997.
(5) Saito, R.; Deesselhaus, G.; Dresselhaus, M. S. *Physical Properties of Carbon Nanotubes*; Imperial College Press: London, 1998.
(6) Terrones, M.; Hsu, W. K.; Hare, J. P.; Kroto, H. W.; Terrones, H.; Walton, D. R. M. *Philos. Trans. R. Soc. London, Ser. A* **1996**, *354*, 2025.
(7) Yakobson, B. I.; Smalley, R. E. *Am. Sci.* **1997**, *85*, 325.
(8) Ajayan, P. M.; Ebbesen, T. W. *Rep. Prog. Phys.* **1997**, *60*, 1025.
(9) Schmid, H.; Fink, H.-W. *Appl. Phys. Lett.* **1997**, *70*, 2679.
(10) Saito, Y.; Hamaguchi, K.; Nishino, T.; Hata, K.; Tohji, K.; Kasuya, A.; Nishina, Y. *Jpn. J. Appl. Phys.* **1997**, *36*, L1340.
(11) Wang, Q. H.; Corrigan, T. D.; Dai, J. Y.; Chang, R. P. H.; Krauss, A. *Appl. Phys. Lett.* **1997**, *70*, 3308.
(12) Dai, L. P. A. T. *Polym. Adv. Technol.* **1999**, *10*, 357.
(13) Chen, Q.; Dai, L.; Gao, M.; Huang, S.; Mau, A. *J. Phys. Chem.* **2001**, *105*, 618.
(14) Ago, H.; Kugler, T.; Cacialli, F.; Salaneck, W. R.; Shaffer, M. S. P.; Windle, A. H.; Friend, R. H. *J. Phys. Chem.* **1999**, *103*, 8116.
(15) Yu, R.; Chen, L.; Liu, Q; Lin, J; Tan, K.-L.; Ng, S. C.; Chan, H. S. O.; Xu, G.-Q.; Hor, T. S. A. *Chem. Mater.* **1998**, *10*, 718.
(16) Mickelson, E. T.; Huffman, C. B.; Rinzler, A. G.; Smalley, R. E.; Hauge, R. H.; Margrave, J. L. *Chem. Phys. Lett.* **1998**, *296*, 188.
(17) Mickelson, E. T.; Chiang, I. W.; Zimmerman, J. L.; Boul, P. J.; Lozano, J.; Liu, J.; Smalley, R. E.; Hauge, R. H.; Margrave, J. L. *J. Phys. Chem. B* **1999**, *103*, 4318.

10.1021/cm040050t CCC: $27.50
Published on Web 11/12/2004

which vary from metals to semiconductors and even to insulators, depending on the type of C−F bonding and the location of the atoms within the carbon network. F-SWNTs have different types of bonding ranging from covalent, semi-ionic, ionic, and even van der Waals interaction because of big electronegativity differences.[22] Therefore, the structure and properties of F-SWNTs have attracted considerable interest.[23−26] Many theoretical calculations have been carried out to predict the electronic and structural properties of F-SWNTs; for instance, fluorinated zigzag tubes are not metallic, the stability and band gap of the fluorinated tubes being dependent upon the fluorination pattern and the tube chirality.[27,28] Experimental results show the increase of resistivity and band gap at high fluorine concentration in the F-SWNTs and fluorinated multiwall carbon nanotubes.[29,30] Therefore, it is very important to control and/or identify the concentration and the fluorination pattern on the fluorinated nanotubes' surface that results from the fluorination processes. It is essential to be able to characterize and predict the surface chemistry associated with fluorinated nanotubes. The motivation for this work is to establish whether core and valence band can distinguish between nanotubes with different structures and fluorine concentration and whether we can use calculation models to explain the observed spectral difference.

In this paper, we report the result of an investigation of carbon SWNTs and F-SWNTs by photoelectron spectroscopy using two photon sources, X-rays (XPS) and UV light (UPS). The experimental valence band and core level spectra were interpreted by spectra generated by CNDO calculations (core spectra) and ab initio molecular orbital calculations (valence band spectra). These calculated spectra assist in the evaluation of the structure and fluorination patterns of F-SWNTs.

Experimental Section

Nanotube Sample. The purified carbon SWNTs and F-SWNTs were prepared by the research group of the late Professor Margrave at Rice University using a previously reported process.[16]

Surface Analysis. All spectra were collected on a VSW HA150 spectrometer (150 mm hemispherical analyzer) operated in the FAT (fixed analyzer transmission) mode with a pass energy of 22 or 44 eV, equipped with a 16 plate multichannel detector system and Al Kα X-radiation (240 W) produced from a 32 quartz crystal VSW monochromator providing an X-ray line width of better than 0.2 eV. The base pressure of the instruments was 10^{-9} Torr or better. The spectrometer energy scales were calibrated[31] using an argon-ion etched copper plate, and all spectra were referenced against the C 1s peak of adventitious hydrocarbon at 284.6 eV. UPS spectra for all samples were obtained using a Specs UVS 10/35 UV source with He II radiation at 40.8 eV. The curve fitting of the XPS spectra was carried out using a nonlinear-least-squares curve-fitting program with a Gaussian/Lorentzian (G/L) product function.[32,33] The Gaussian/Lorentzian mixture was taken as 0.5.

Calculations. The ab initio closed-shell restricted Hartree−Fock calculations were performed using the Gaussian 98W program on a PC and a minimal STO-3G type basis set using single multiplicity and then were refined using an 3-21G type extended basis set[34] for all of the calculations. CNDO calculations were conducted using a program developed by one of us and reported earlier,[35] whose input geometry was optimized by Gaussian 98W based upon the minimization of energy. This program was used to perform relaxation potential model and electronic charge calculations for the atoms of the nanotube molecule. The chemical shift of the carbon atom was calculated on the basis of the relaxation potential model (RPM) using the CNDO atomic charges, Mann's integrals[36] for the $\langle 1/r \rangle$, and relaxation energies calculated using one-half the difference in electronic potential for the molecule, and the molecule with the atom of interest replaced by the atom of atomic number greater by one.[35,37,38] The calculated valence band spectra were obtained from ab initio molecular orbital calculations by the addition of the component peaks for each calculated energy level where the position of each peak corresponded to the theoretical energy level. The intensity of each component peak was given by the net atomic population of the energy level, adjusted by the level's photoelectron cross-section, as published by Scofield[39] for XPS and by Yeh and Lindau for UPS.[40] Each peak in the calculated spectrum has the same full-width at half-maximum (fwhm) and a G/L mixing ratio of 0.5.[32] The peak fwhm was set to a chosen value for best comparison with the experimental spectra (specific values are given below). This approach has been successively applied to other polymer systems.[41,42]

Results and Discussion

XPS Analysis of SWNT and F-SWNT. *Survey Spectra.* Figure 1 (I) shows the overall (survey) spectra for the SWNTs and F-SWNTs. A dominant C 1s peak

(18) Okotrub, A. V.; Bulusheva, L. G.; Yudanov, N. F.; Chuvilin, A. L.; Romanenko, A. I.; Asanov, I. P.; Shubin, Y. V.; Yudanova, L. I. In *Chemistry and Physics of Fullerenes and Carbon Nanomaterials*; Kamat, P. V., Guldi, D. M., Kadish, K. M., Eds.; Electrochemical Society Proceedings: 2000; Vol. 2000-10, pp 255−261.
(19) Touhara, H.; Okino, F. *Carbon* **2000**, *38*, 241.
(20) Hayashi, T.; Terrones, M.; Scheu, C.; Kim, Y. A.; *Ruhle*, M.; Nakajima, T.; Endo, M. *Nano Lett.* **2002**, *2*, 491.
(21) Zhao, W.; Song, C.; Zheng, B.; Liu, J.; Viswanathan, T. *J. Phys. Chem. B* **2002**, *106*, 293.
(22) Tressaud, A.; Guimon, C.; Gupta, V.; Moguet, F. *Mater. Sci. Eng., B* **1995**, *30*, 61.
(23) Plank, N. O. V.; Cheung, R. *Microelectron. Eng.* **2004**, *73−74*, 578.
(24) Lee, Y. S.; Cho, T. H.; Lee, B. K.; Rho, J. S.; An, K. H.; Lee, Y. H. *J. Fluorine Chem.* **2003**, *120*, 99.
(25) Peng, H.; Reverdy, P.; Khabashesku, V. N.; Margrave, J. L. *Chem. Commun.* **2003**, *3*, 362.
(26) Bettinger, H. F.; Kudin, K. N.; Scuseria, G. E. *J. Am. Chem. Soc.* **2001**, *123*, 12849.
(27) Park, K. A.; Choi, Y. S.; Lee, H. Y.; Kim, C. *Phys. Rev. B* **2003**, *68*, 045429.
(28) Kudin, K. N.; Bettinger, H. F.; Scuseria, G. E. *Phys. Rev. B* **2001**, *63*, 045413.
(29) An, K. H.; Heo, J. G.; Jeon, K. G.; Bae, D. J.; Jo, C.; Yang, C. W.; Park, C. Y.; Lee, Y. H.; Lee, Y. S.; Chung, Y. S. *Appl. Phys. Lett.* **2002**, *80*, 4235.
(30) An, K. H.; Park, K. A.; Heo, J. G.; Lee, J. Y.; Jeon, K. K.; Lim, S. C.; Yang, C. W.; Lee, Y. S.; Lee, Y. H. *J. Am. Chem. Soc.* **2003**, *125*, 3057.
(31) Seah, M. P. *Surf. Interface Anal.* **2001**, *31*, 721.
(32) Sherwood, P. M. A. Auger and X-ray Photoelectron Spectroscopy. In *Practical Surface Analysis*, 2nd ed.; Briggs, D., Seah, M. P., Eds; Wiley: Chichester, 1990; Vol. 1, Appendix 3.
(33) Ansell, R. O.; Dickinson, T.; Povery, A. F.; Sherwood, P. M. A. *Electroanal. Chem*. **1979**, *98*, 79.
(34) Dupuis, M.; Farazdal, A.; Karna, S. P.; Maluends, S. A. In *Modern Techniques in Computational Chemistry: MOTECC-90*; Clement, E., Ed.; Escom: Leiden, 1990; Chapter 6, pp 277−342.
(35) Sherwood, P. M. A. *J. Chem. Soc., Faraday Trans. 2* **1976**, *72*, 1791.
(36) Mann, J. B. *Atomic Structure Calculations. II Hartree−Fock Wave functions and Radial Exception Values: Hydrogen to Lawrencium*; Los Alamos Scientific Laboratory: Los Alamos, NM, 1968.
(37) Davis, D. W.; Banna, M. S.; Shirley, D. A. *J. Chem. Phys*. **1974**, *60*, 237.
(38) Davis, D. W.; Shirley, D. A. *J. Electron Spectrosc.* **1974**, *3*, 137.
(39) Scofield, J. H. *J. Electron Spectrosc. Relat. Phenom*. **1976**, *8*, 129.
(40) Yeh, J. J.; Lindau, I. *At. Data Nucl. Data Tables* **1985**, *32*, 7.
(41) Hamilton, L.; Sherwood, P. M. A.; Reagan, B. M. *Appl. Spectrosc*. **1993**, *47*, 139.
(42) Viswanathan, H.; Wang, Y.-Q.; Audi, A. A.; Allen, P. J.; Sherwood, P. M. A. *Chem. Mater.* **2001**, *13*, 1647.

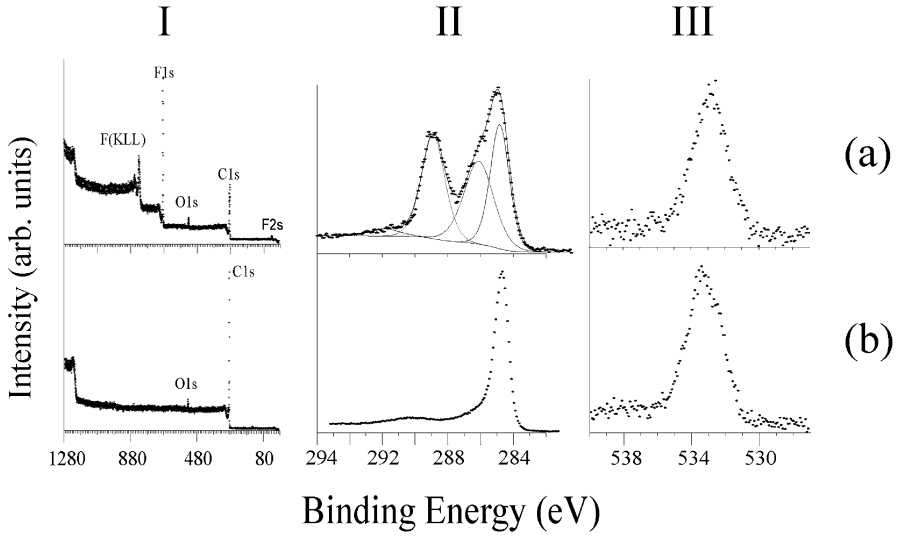

Figure 1. XPS survey spectra (I), C 1s (II), and O 1s (III) of F-SWNTs (a) and SWNTs (b).

(binding energy 284.6 eV) was shown in the spectra of both samples. In the spectrum of F-SWNTs, an intense F 1s feature is seen with a binding energy of 688 eV together with intense F Auger peaks around 830 eV. A low intensity O 1s feature with a binding energy of 530 eV due to chemisorbed oxygen is seen in the spectra of both samples. The relative intensity of this O 1s feature is significantly greater than that seen in our studies of untreated carbon fibers and HOPG.[43,44] Furthermore, the intensity of O 1s in the F-SWNTs is higher than that in SWNTs (vide infra).

C 1s Region. The C 1s region XPS spectra for SWNTs and F-SWNTs are shown in Figure 1 (II) where the spectrum of the fluorinated sample was curve-fitted. The SWNTs give a single C 1s peak at 284.6 eV, which corresponds to the principal carbon peak (similar to the graphitic peak of graphite), together with a very weak and wide peak around 290 eV due to $\pi\sim\pi$ shake up processes, resulting from the extensive π-character in carbon nanotubes. The F-SWNTs give a multicomponent C 1s spectrum which we have fitted to four components, one at 284.6 eV due to the carbon atoms unattached to and at more than two atoms away from fluorine atoms, one at 285.8 eV corresponding to carbon atoms separated from a fluorine atom by another carbon atom, and the other two peaks at 288.8 and 290.8 eV due to carbon atoms directly connected to fluorine atoms.

O 1s Region. The O 1s region XPS spectra for SWNTs and F-SWNTs are shown in Figure 1 (III). There is little asymmetry in the O 1s region, and we have not curve-fitted the spectra. The area ratio of the C 1s region and the O 1s region is used to calculate the atomic ratio of carbon and oxygen based upon the approximation that the region is homogeneous and using Scofield cross sections.[39] The O/C ratio for SWNT is 0.026, and for F-SWNT it is 0.148. This ratio is somewhat higher than the ratio 0.016 typical of unoxidized carbon (graphite and carbon fibers[43]) where chemisorbed oxygen is the main source of oxygen. The higher levels of oxygen on the nanotubes are probably caused by the higher surface area for these sample than the other sources of graphite. The F-SWNTs have a more active surface than the SWNTs because of the presence of the electronegative fluorine atoms on the surface of the nanotubes, leading to a much higher level of chemisorbed oxygen.

F 1s Region and Auger. Fluorine was, as expected, only detected in the F-SWNT sample, the F 1s and fluorine KLL Auger region being shown in Figure 2 (I). The F 1s peak comes at comparable binding energies for CF_x species with different values of x, the C 1s peak, however (as seen in Figure 1 (III)), being found at different binding energies. The one F 1s peak at 687.2 eV is compatible with the binding energy of fluorinated graphite (C_4F).[45] The kinetic energy of the KLL Auger peaks was observed at 610.3 eV for KL_1L_1, 628.7 eV for L_1L_{23}, and 655.2 for $KL_{23}L_{23}$. The $KL_{23}L_{23}$ kinetic energy is about 1.5 eV lower than that of the fluorinated graphite sample (656.7 eV).[45] The area ratio of the C 1s region and the F 1s region is used to calculate the atomic ratio of carbon and fluorine based upon the approximation that the region is homogeneous and using Scofield cross sections as in the case of the O 1s region.[39] The atomic C/F ratio was about 3.62.

XPS Valence Band. The valence band region has the potential to distinguish subtle differences in surface chemistry, and these differences can be understood by comparison of the experimental spectrum with a calculated spectrum.[46] The valence band XPS spectra for the SWNTs and F-SWNTs are shown in Figure 2 (II). The SWNT spectrum is dominated by an intense C 2s region around 18 eV and a broad C 2p region in the range 9−15 eV. There is only a weak O 2s region around 26 eV consistent with the oxygen found in the O 1s region being associated with chemisorbed oxygen, as the valence band region is more bulk sensitive due to the higher kinetic energy and larger escape depth of the valence band electrons. Oxidized carbon shows an intense O 2s region.[43] The valence band spectrum of F-SWNTs shows an intense peak at 33 eV due to F 2s

(43) Wang, Y.-Q.; Zhang, F.-Q.; Sherwood, P. M. A. *Chem. Mater.* **1999**, *11*, 2573.
(44) Xie, Y.; Sherwood, P. M. A. *Surf. Sci. Spectra* **1993**, *1*, 253.
(45) Wagner, C. D.; Riggs, W. M.; Davis, L. E.; Moulder, J. E. *Handbook of X-ray Photoelectron Spectroscopy*; Perkin-Elmer Corp.: 1979.
(46) Sherwood, P. M. A. In *Surface Analysis by Auger and X-ray Photoelectron Spectroscopy*; Briggs, D., Grant, J. T., Eds.; Surface Spectra Ltd. and IM Publications: Chichester, 2003; Chapter 19, pp 531−555.

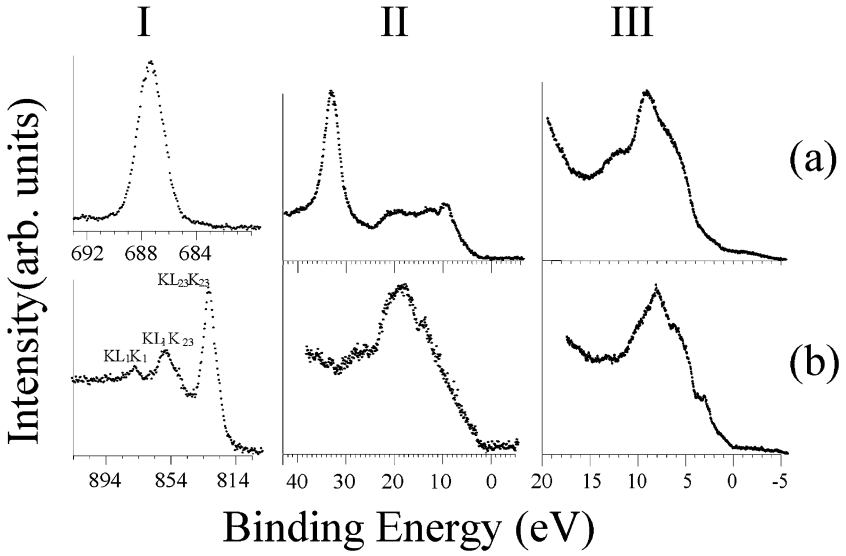

Figure 2. XPS F 1s (a) and Auger spectra (b) of F-SWNTs (I), XPS valence band spectra (II), and UPS spectra (III) of F-SWNTs (a) and SWNTs (b).

which has a high photoelectron cross section. F 2p features, which are of much lower cross section than F 2s features, appear around 6−12 eV, but the higher cross section of F 2s and F 2p as compared to C 2s and C 2p causes fluorine features to dominate the spectrum.

UPS Analysis of SWNTs and F-SWNTs. UPS is much more surface sensitive than XPS because the electrons have a much lower kinetic energy as a result of the much smaller photon energy (40.8 eV for He(II) rather than 1486.6 eV for AlKα X-radiation). The valence band He(II) UPS spectra for SWNTs and F-SWNTs are shown in Figure 2 (III). The valence band spectra are determined by the fact that the p orbital of carbon and fluorine has a higher photoelectron cross section than the s orbital for the He II radiation. The F 2p cross section is much higher than the C 2p cross section, so that the F-SWNT spectrum is dominated by fluorine. An added uncertainty in the analysis of these spectra is the extent to which the spectra may depend on the joint density of states of the initial and final states.

Calculation of the Preferred Structures of Normal and Fluorinated Nanotubes. A carbon nanotube can be regarded as the rolling of a graphite sheet (graphene) in a certain direction, leading to the formation of different chiralities of nanotube. The nanotube can be defined by the chiral vector (n, m). If n is equal to m, the nanotube is called an "armchair" nanotube, while if $m = 0$, the nanotube is called a "zigzag" nanotube. This means that different sizes of original graphene sheet make various kinds of nanotubes with different properties. Certain nanotubes show the properties of conductors, and some are semiconductors. These observations have been supported by theoretical and experimental studies.[47−51] To simplify the calculations and discussion, only "zigzag" and "armchair" nanotubes are considered.

Structural Analysis of Normal Nanotubes. Figure 3 shows the tube skeleton and the bond lengths that were obtained for normal nanotube models where the carbon skeleton is terminated by hydrogen atoms. The top inset to the figure illustrates the two types of nanotube whose tube axis is indicated by the arrow. The lower insets show the "zigzag" nanotube is represented by the $C_{32}H_8$ structure and the "armchair" nanotube is represented by the $C_{30}H_{12}$ structure. Actual nanotubes do not normally have hydrogen present, and the hydrogen atoms were added to terminate the small units used to represent the nanotube structure to give a neutral molecule. The three structures of increasing (left to right) nanotube diameter for the "zigzag" nanotube are on the left, and the five structures of the "armchair" nanotube of increasing nanotube diameter are on the right. Two bond lengths can be identified; bond length B1 lies along the tube axis in a "zigzag" nanotube, and perpendicular to the tube axis in an "armchair" nanotube. The remaining two bonds, B2 and B3, lie at approximately 60° to the B1 bond. The results for B3 are nearly identical to those for B2, and so only B2 is shown in Figure 3. The bond lengths shown in Figure 3 correspond to the lengths obtained for the minimum energy configuration obtained using ab initio calculations with a 3-21G basis set.

Zigzag Tube. The length of the B1 C−C bond (parallel to the tube axis) was found to increase as the cluster chosen corresponded to an increasing nanotube diameter. The lengths of the other bonds (B2 and B3) become shorter as the nanotube diameter increased. When the size of the tube is large enough, B1 and B2 become very close to the bond length of graphite (about 1.43 Å).

Armchair Tube. The length of the B1 C−C bond (perpendicular to the tube axis) was found to decrease as the cluster chosen corresponded to increasing nanotube diameter. The length of the other bonds (B2 and B3) increased until B1 and B2/B3 both became around 0.143 nm, the bond length in a graphite crystal.

The rolling of the graphene sheet into a nanotube will induce the strain on the skeleton which is closely related

(47) Chen, Q.; Dai, L.; Gao, M.; Huang, S.; Mau, A. *J. Phys. Chem.* **2001**, *105*, 618.
(48) Hamada, N.; Swada, S.; Oshiyama, A. *Phys. Rev. Lett.* **1992**, *68*, 1579.
(49) Wildoer, J. W. G.; Venema, L. C.; Rinzler, A. G.; Smalley, R. S.; Dekker, C. *Nature* **1998**, *391*, 59.
(50) Odom, T. W.; Huang, J.-L.; Kim, P.; Lieber, M. C. *Nature* **1998**, *391*, 62.
(51) Ebbsen, T. W.; Lezec, H. J.; Hiura, H.; Bennett, J. W.; Ghaemi, H. F.; Thio, T. *Nature* **1996**, *382*, 54.

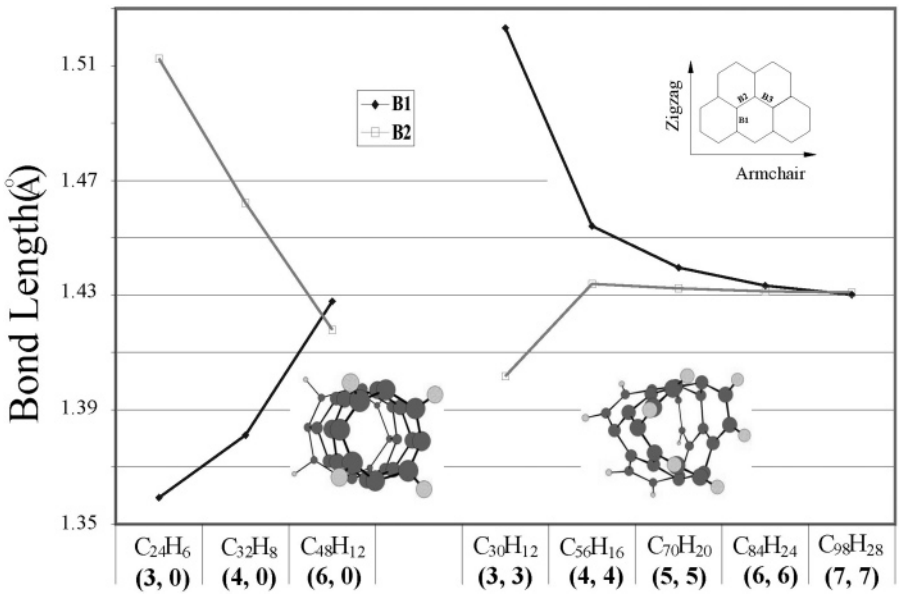

Figure 3. Bond length of SWNTs optimized by Gaussian 98W at the 3-21G basis set; the right part is zigzag type, and the left side is armchair type.

to the tube size.[52,53] This is why when the tube diameter (or size) is small, the bond length perpendicular to or laying at an angle to the tube axis is always larger than the other bond length. When the tube diameter is large, the effect is very small, the length values of B1 and B2 bonds become much closer, and the ring becomes more symmetrical. Consequently, the chemistry of the large diameter nanotube should be similar to that of graphite, whereas the small diameter nanotubes are expected to be more chemically reactive because of the higher strain in the carbon skeleton.

Structural Analysis of Fluorinated Nanotubes. Previous studies show that the fluorination process of SWNTs leads to F-SWNTs with different carbon-to-fluorine ratios, corresponding to different numbers of fluorine atoms covalently attached to the side-wall of the SWNTs. The stoichiometries of the tubes fluorinated by reacting SWNTs with gaseous fluorine agent at 150°, 250°, 325°, and 400 °C were $CF_{0.10}$, $CF_{0.46}$, $CF_{0.55}$, and $CF_{0.65}$, respectively, determined by electronic microprobe analysis.[16] A reaction temperature of over 150 °C was necessary for fluorine to be attached covalently to the tube. It is necessary to have a C_2F limiting stoichiometry to maintain the tubelike structure for the fluorinated nanotubes.[16] It is interesting to note that the unfluorinated SWNTs can be obtained by reacting the fluorinated F-SWNTs with anhydrous hydrazine, which implies that the fluorinated tube is a tubelike structure and not in the thermodynamically most stable phase. It was believed that the fluorine atoms are attached to the outside of the tube. The fluorinated nanotubes ambiguously are of shorter length and much lower electrical conductivity. In this paper, the stoichiometries of zigzag C_2F, C_3F, and C_4F are used to represent the F-SWNTs. These stoichiometries correspond to the presence of $\ni$CF and not $>CF_2$ or $-CF_3$ functionality, for the latter functionalities would cause holes in the structure and a breakdown of the tube arrangement, except in the case of functionality at the ends of the tube.

Scheme 1. The Distribution Patterns of Fluorine Atoms in a C_2F-type Nanotube[a]

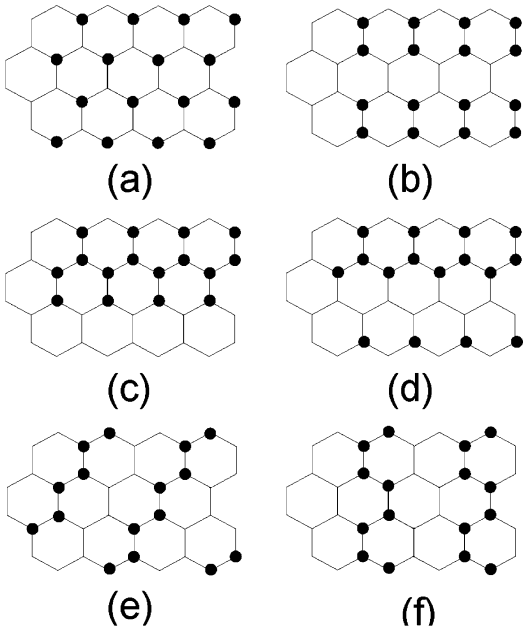

[a] The big dot represents the carbon atom connected to fluorine.

C_2F. In the case of C_2F, a number of arrangements are possible where the fluorine atoms are attached in various zigzag arrangements by covalent bonding to the nanotube, and six arrangements are represented in Scheme 1. In Scheme 1, we have chosen the (4,0) zigzag arrangement as a simple manifestation of the zigzag arrangement. In drawings (a) and (b), the C−F bonds lead to a π-bond arrangement that is separated and localized; in other words, there is no extended π-system. In drawings (c) and (d), the fluorine atoms are arranged in a pattern that allows some extended π-bonds to be formed perpendicular to the tube axis, but not along the

(52) Mintmire, J. W.; White, C. T. In *Carbon Nanotubes*; Ebbesen, T. W., Ed.; CRC Press: Boca Raton, FL, 1997.
(53) Hernandez, E.; Goze, C.; Bernier, P.; Rubio, A. *Appl. Phys. A* **1999**, *68*, 287.

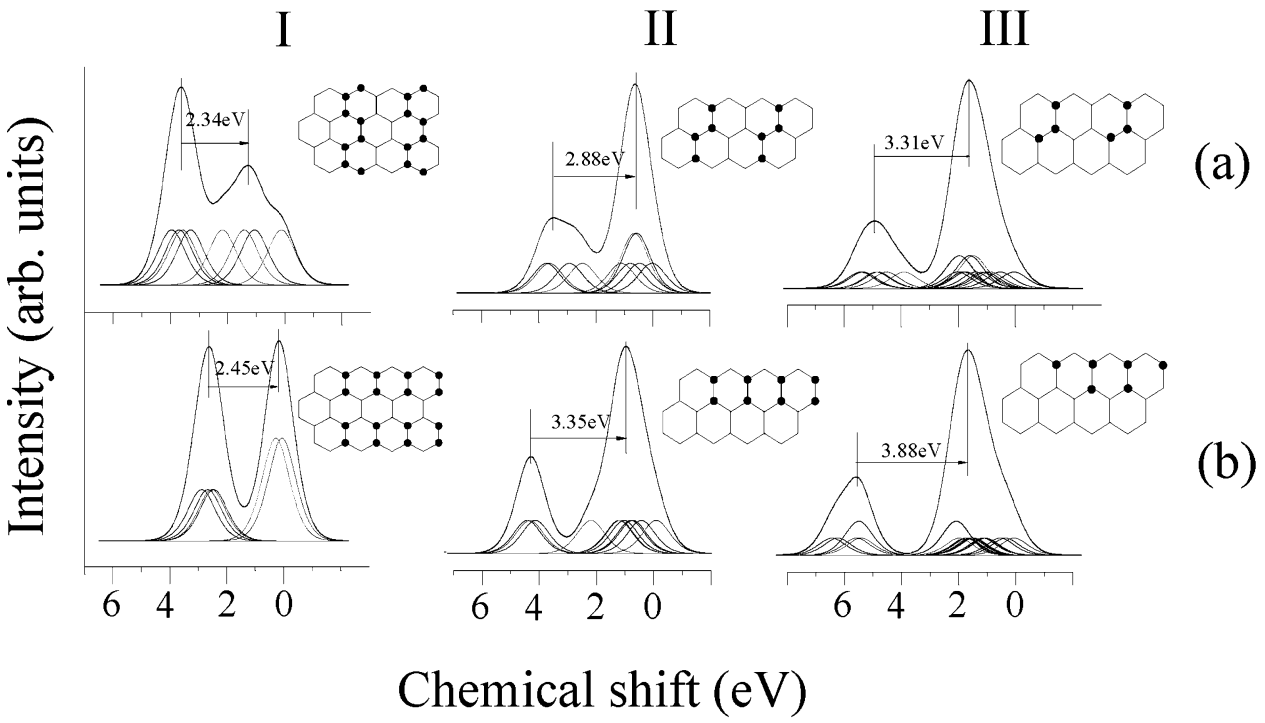

Figure 4. Synthetic C 1s spectra of F-SWNTs with various stoichiometries and distribution patterns of fluorine from calculation, showing the chemical shift (fwhm = 0.6 eV). I, C_2F; II, C_3F; III, C_4F. The dark dots are carbon connected to fluorine. (a) Conductive pattern; (b) nonconductive pattern.

axis. In drawings (e) and (f), the fluorine atoms are in a pattern that allows the remaining carbon atoms to form continuous overlapping π-bonds along the tube axis, leading to an electronically conducting structure with some electrical resistance as compared to SWNTs as a result of the C−F bonds in the structure. The attachment of fluorine to carbon causes the sp^2-type bonds of SWNTs to be replaced by sp^3-type bonds for those carbon atoms connected directly to fluorine, leading to a strained structure with some shorter and some longer bonds.

Calculations were performed on three fluorinated nanotubes based upon the $C_{32}F_{16}H_8$, and the bond lengths were compared to the $C_{32}H_8$ SWNT. These F-SWNT structures were based upon the (b), (e), and (f) configurations shown in Scheme 1. The bond lengths that will now be discussed correspond to the lengths obtained for the minimum energy configuration obtained using ab initio calculations with a 3-21G basis set. These calculated bond lengths show that the lengths of C−C bonds that do not lie along the tube axis and that are attached to fluorine atoms are longer (0.158 nm for configuration (f)) than the same bonds that not attached to fluorine (0.147 nm). The calculations also show that the lengths of C−C bonds lying along the tube axis that are attached to fluorine atoms are also longer (0.152 nm for configuration (f)) than the same bonds that are not attached to fluorine (0.132 nm). The C−F bond was unaltered for the different configurations at around 0.1375 nm. The F-SWNT structures of the lowest energy were bent and tangled.

C_3F and C_4F. For the C_3F and C_4F stoichiometries, there are more than six possible distributions of fluorine atoms onto the (4, 0) zigzag nanotube. We have optimized the geometry of only a few of the possible arrangements, and the chosen geometries are shown as an inset in Figures 4 and 8. For C_3F, three $C_{24}F_8H_8$ structures were examined based upon the $C_{24}H_6$ zigzag nanotube shown in Figure 7. Two of these three $C_{24}F_8H_8$ structures are shown schematically in Figure 4. When the geometries were optimized, it was found that the bond lengths were considerably changed from the corresponding unfluorinated nanotube with most of the bond lengths being longer. The bond length of the C−C bonds which are connected to fluorine and were parallel to the tube axis changed by the largest amount, from 0.136 nm in the unfluorinated nanotube to between 0.155 and 0.164 nm in the three fluorinated nanotube structures. The length of the C−C bond perpendicular to the axis and connected to carbon that was attached to fluorine showed a much smaller increase (no more than 0.04 nm). The C−C bond length for carbon atoms that were not attached to fluorine had a bond length between 0.148 and 0.130 nm in the three chosen structures. The C−F bond length was longer than that found for the C_2F configurations being around 0.140 nm. The strain that is introduced into the nanotube by the attachment of fluorine atoms is known to lead to nanotubes that are less stable than the unfluorinated nanotubes, explaining the known decomposition of the fluorinated nanotubes by loss of fluorine gas to give unfluorinated nanotubes.[16]

Three C_4F nanotube $C_{24}F_6H_8$ structures were examined based upon the $C_{24}H_8$ zigzag nanotube. The optimized geometries showed changes similar to those found for the C_3F nanotubes. All of these results are similar to those from other calculations, although other calculations have not focused on the interpretation of the core level and valence band photoelectron spectra.

The Calculation of the Chemical Shift of Carbon Atoms in the Fluorinated Nanotube. XPS studies of the C 1s core region show substantial chemical shifts for

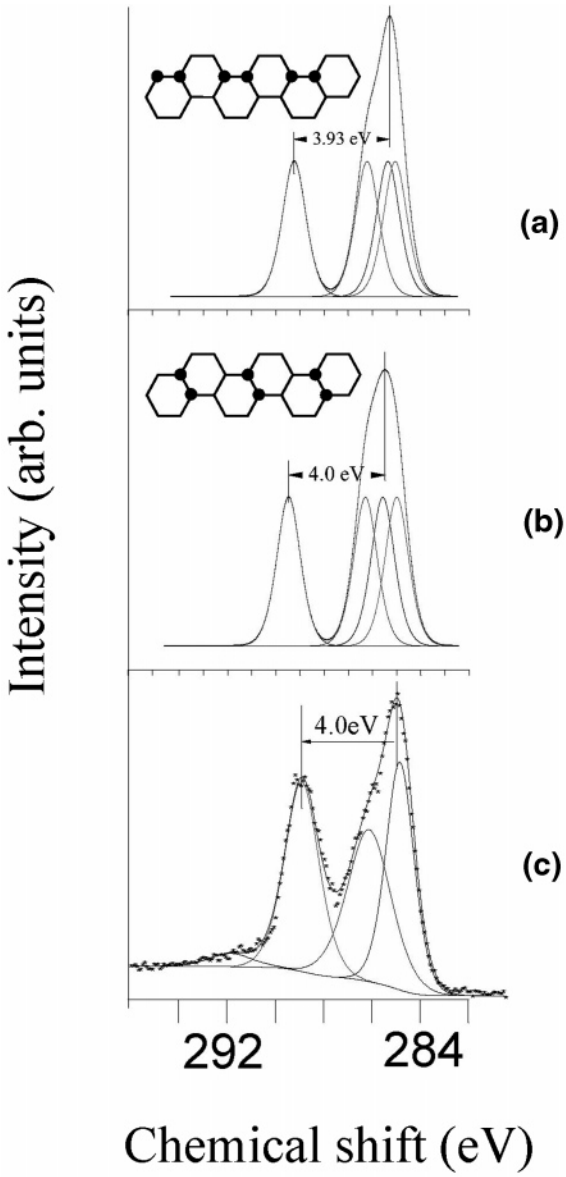

Figure 5. Comparison of synthetic (a, b) with experimental (c) C1s spectra of F-SWNTs, showing similar chemical shifts and spectrum shapes (fwhm = 0.6 eV).

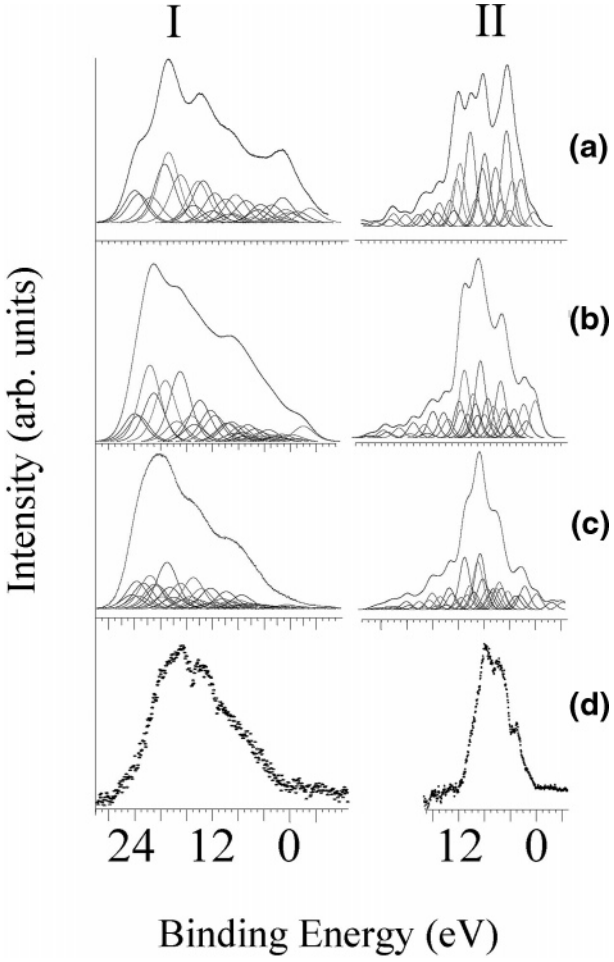

Figure 6. XPS and UPS valence band spectra of SWNTs. I, XPS (fwhm = 1.5 eV); II, UPS (fwhm = 1 eV); (a) (3, 0) zigzag, (b) (4, 0) zigzag; (c) (6, 0) zigzag SWNTs, and (d) experimental.

fluorinated hydrocarbons, making core XPS a valuable approach for the examination of the surface chemistry of fluorinated carbon compounds. The relaxation potential method (RPM)[35,38] and the references therein have been successfully applied to the interpretation of core XPS binding energies for the past 30 years, and we have used this approach to predict the binding energies and thus the expected spectrum for the C_2F, C_3F, and C_4F nanotube structures that we have discussed above.

Calculated C 1s Spectra for Zigzag Nanotubes. Figure 4 shows the spectra calculated for two of the six C_2F, two of the three C_3F, and two of the three C_4F structures for the (4,0) zigzag nanotube discussed above. In each case, the structure in (a) is a conducting nanotube and the structure in (b) is a nonconducting nanotube, based on the localization of the π-bond mentioned above. It is interesting to note that there are some significant differences in the appearance of the calculated spectra; in particular, the separation and relative intensities of the two principal peaks change considerably, depending on the C/F ratio and fluorination pattern in the fluorinated nanotubes. Table 1 shows the calculated chemical shift and relaxation energy of the carbon atom with the greatest chemical shift in the fluorinated nanotube using both the ground state potential model (GPM) and the RPM model. The calculated differences in the GPM chemical shift, the extraatomic relaxation energy, and RPM chemical shift are shown. These differences are relative to the carbon atom with the lowest binding energy. The calculated spectra in Figure 4 show the chemical shifts calculated for all of the carbon atoms, but Table 1 shows only the carbon atom of highest binding energy to simplify the table. It can be seen that the RPM chemical shift of the carbon atom illustrated in Table 1 increases in going from C_2F to C_4F, while this is not the case for the GPM. The significant differences in the relaxation energy lead to the overall trend predicted by the GPM calculation.

The calculated spectra clearly show that the structure of the nanotube can have a significant effect on the appearance of the C 1s core region. It is important to note that the need to use hydrogen atoms to terminate the molecule used to represent the nanotube has an impact on the calculated relaxation energy. This is because the electronegative nature of fluorine leads to lower C 1s relaxation energies as a result of the reluctance of electron density on the fluorine to be

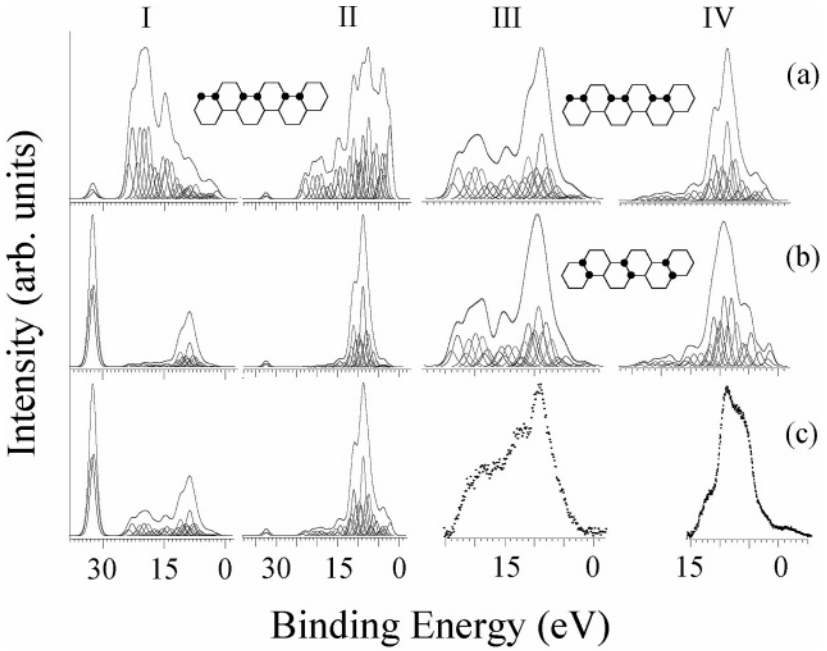

Figure 7. (I) Contribution of carbon (I(a)) and fluorine (I(b)) to the XPS valence band (I(c) = I(a) + I(b)) of (3, 3) armchair F-SWNTs. (II) Contribution of carbon (II(a)) and fluorine (II(b)) to the UPS valence band (II(c) = II(a) + II(b)) of F-SWNTs. (III) Comparison of the XPS out valence band of calculated III(a) and III(b) with experimental data III(c) of F-SWNTs. (IV) Comparison of UPS spectra of calculated IV(a) and IV(b) with experimental data IV(c) of F-SWNTs.

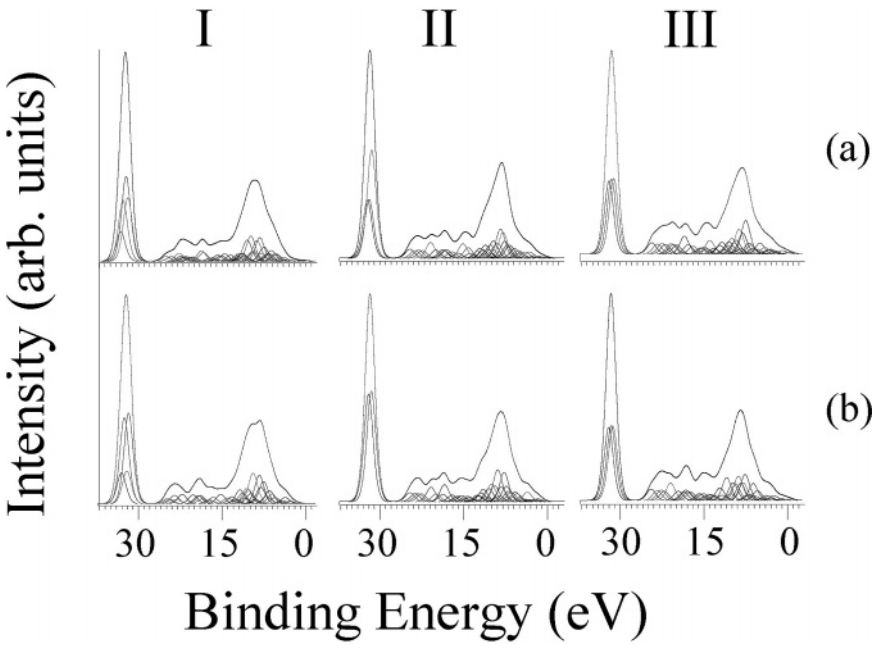

Figure 8. Calculated VB spectra of F-SWNTs with various stoichiometries and distribution pattern of fluorine. I, C_2F; II, C_3F; III, C_4F. (a) Conductive pattern; (b) nonconductive pattern. The structures used here are the same as those in Figure 8.

involved in the relaxation process. The electron from the hydrogen atom will be more involved in the relaxation process, so that the use of terminating hydrogen atoms will lead to a calculated relaxation energy that would be expected to be less than the experimental value. The effect of this is to give the asymmetry on the low-binding energy side of the calculated spectrum caused by too small a chemical shift as a result of the use of terminating hydrogen atoms for the carbon atoms in this chemical shift range.

Calculated C 1s Spectra for Armchair Nanotubes. Figure 5 shows the spectra calculated for two (3,3) fluorinated armchair nanotubes of composition $C_{24}F_6H_8$. The structure in (b) is a conducting nanotube, and the structure in (a) is a nonconducting nanotube.

Comparison of the Calculated and Experimental C 1s Spectra. There is no other experimental data available for the C 1s XPS region of C_2F nanotubes, although data for fluorinated graphite with a C_2F composition have been published.[18] The separation of the main peaks characterized by XPS was about 2.45 eV, and its spectral shape can be seen to be similar to the calculated spectrum (Figure 4 I(a)). For the C_3F fluorinated nanotube published in the literature,[18] the peak separation was about 3.35 eV, which is in good agreement with the calculated spectrum discussed above for the zigzag C_3F

Table 1. Calculated Chemical Shift and Relaxation Energy of the Carbon Atom with the Greatest Chemical Shift in the Fluorinated Nanotubes[a]

		Δchemical shift_{GPM}	Δrelaxation energy	Δchemical shift_{RPM}
C_2F	(a)	2.02	2.05	3.83 (2.34)
	(b)	2.11	1.48	2.82 (2.45)
C_3F	(a)	2.21	2.31	3.69 (2.88)
	(b)	4.05	4.50	5.29 (3.35)
C_4F	(a)	2.80	3.37	5.36 (3.31)
	(b)	2.94	4.38	6.38 (3.88)

[a] Note: The number in parentheses is the separation between the peak maxima of the two principal peaks in the calculated spectra. The principal peaks are composed of the overlap between a number of component peaks.

pattern nanotubes, and also the experimental spectral shape is very close to the calculated spectrum (Figure 4 II(b)), which implies that the fluorine distribution on the fluorinated nanotubes obtained in that work is very similar to the fluorination pattern shown in Figure 4 II(b). For the fluorinated nanotube in this research, the C/F atomic ratio was about 3.6, with the principal peaks separated by about 4.0 eV. The relative intensity of the two principal peaks (Figure 1 (II)) corresponded to a higher relative intensity for the high binding energy peak. The best agreement between the calculated spectra and the experimental spectra is obtained for the C_4F armchair nanotubes, and Figure 5 shows the very good agreement in the width and separation of the principal peaks between the calculated and experimental spectra. The asymmetry of the low binding energy peak seen experimentally is predicted in the calculated spectra.

The experimental spectra show a very low intensity feature with a binding energy of 292 eV which is not predicted in the calculated spectra. The chemical shift of this feature from the first principal peak is about 7.4 eV. This high binding energy is too large for a ∋CF feature and is consistent with the presence of $>CF_2$ functionality. We believe that the $>CF_2$ functionality arises from fluorination at the end of the tube. If this is correct, the relative intensity of this feature is an indication of the length of the tube, and we believe that the fluorination process leads to a shortening of the tube length.

The comparisons between the calculated and experimental data discussed above show that the fluorine atoms appear to favor bonding to existing fluorine atoms, which was predicted by previous workers using the ONIOM calculation method.[54] The differences seen in the calculated spectra among different C/F ratios and fluorination patterns suggest that the C 1s region spectrum can be used as a means of identification of the structure of normal and fluorinated nanotubes.

The Calculation of XPS Valence Band and UPS Spectra. Valence band XPS has the potential to distinguish subtle chemical differences in carbon surface chemistry.[46,55] Figure 6 compares the experimental XPS and He(II) UPS valence band spectra for unfluorinated nanotubes with spectra calculated for the three zigzag structures of Figure 3. It can be seen that the spectral features in the XPS and UPS spectra become narrower as the number of carbon atoms in the nanotube increases, (a) $C_{24}H_6 \rightarrow$ (b) $C_{32}H_8 \rightarrow$ (c)$C_{48}H_{12}$. Comparison of the experimental spectra with the calculated spectra of normal carbon nanotubes indicates that the best agreement between theory and experiment is obtained for the zigzag structure represented by Figure 6c, the $C_{48}H_{12}$ nanotube. Figure 7 compares the experimental XPS and He(II) UPS valence band spectra for fluorinated nanotubes with spectra calculated for the two armchair structures whose C 1s region was shown in Figure 5. The right-hand side of the figure shows the calculated and background subtracted experimental spectra for the outer valence band region, and the left-hand side of the figure shows how the overall spectrum (c) is composed of a carbon (a) and fluorine (b) contribution. The intense F 2s region in the XPS spectrum (shown in Figure 2 (II)) with a binding energy of about 32 eV is predicted in the calculation. The calculation also shows a very low intensity F 2s region in the UPS spectrum due to the low F 2s cross section for UV light. The UPS spectrum in the outer valence band region is dominated by the high F 2p cross section. The principal differences in the valence band are seen in the outer valence band region on the right-hand side of Figure 7. The left-hand side of the figure shows that the principal carbon contributions are mainly the C 2s features at a binding energy greater than 15 eV and F 2p features at a binding energy less than 15 eV. Because we have seen that the fluorine is largely in the form of ∋CF bonds, we would not expect much difference in the mainly F 2p region, but we would expect some significant differences in the mainly C 2s region. Both of the calculated spectra in Figure 7 show good agreement with experiment.

Figure 8 shows the calculated valence band spectra for the zigzag nanotubes, but in this case the agreement between theory and experiment is not as good as it was for the armchair nanotubes in this research.

Conclusions

This study shows that core and valence band photoelectron spectroscopy can be valuable in understanding the structure and composition of nanotubes, especially fluorinated nanotubes. Core and valence band spectra assist in the identification of the main features in the experimental spectra and suggest that the fluorinated nanotubes studied in this work are most likely in the armchair configuration. The calculations provide a set of calculated spectra that should assist in the interpretation of photoelectron spectra of different nanotube structures. In particular, the C 1s region would be expected to show significant differences for different fluorinated nanotube structures, with the C_2F nanotube with the smallest separation between the two principal peaks seen in the C 1s region (2.3−2.5 eV), C_3F at an intermediate separation (2.9−3.4 eV), and C_4F with the largest peak separation (3.3−4.0 eV). The conducting nanotubes correspond to the first number in parentheses and the insulating nanotubes are the second number, corresponding to a greater separation between the principal features in the C 1s region for the insulating nanotubes. Based on this result, the fluorination pattern and chemical ratio of fluorinated carbon nanotubes can be understood by interpretation of the C1s spectrum and valence band spectrum.

(54) Bauschlicher, C. W., Jr. *Chem. Phys. Lett.* **2000**, *322*, 237.
(55) Sherwood, P. M. A. Nanostructured Composites Using Carbon-Derived Fibers. In *Dekker Encyclopedia of Nanoscience and Nanotechnology*; Marcel Dekker Inc.: New York, in press.

Acknowledgment. We thank the late Professor John L. Margrave, E.D. Butcher Professor of Chemistry at Rice University, who provided the nanotubes that were used in this study. He would have been a coauthor of this paper, but his recent death meant that he was neither able to see the manuscript nor discuss the results of the study. This material is based upon work supported by the National Science Foundation under Grant CHE-0137502. The U.S. Government has certain rights in this material.

CM040050T